ORIGINAL PAPER



The structure of *Vibrio cholerae* FeoC reveals conservation of the helix-turn-helix motif but not the cluster-binding domain

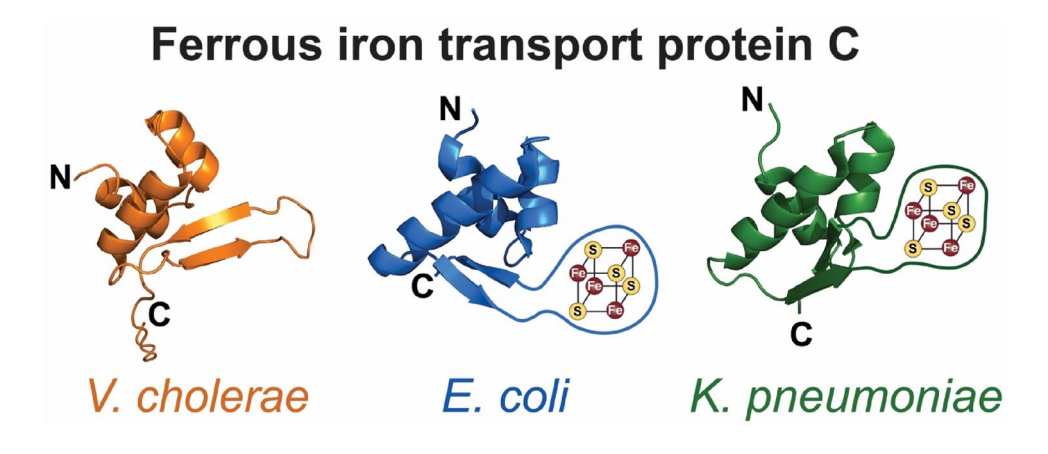
Janae B. Brown¹ · Mark A. Lee¹ · Aaron T. Smith¹

Received: 28 February 2022 / Accepted: 4 June 2022 / Published online: 7 July 2022 © The Author(s), under exclusive licence to Society for Biological Inorganic Chemistry (SBIC) 2022

Abstract

Most pathogenic bacteria require ferrous iron (Fe²⁺) in order to sustain infection within hosts. The ferrous iron transport (Feo) system is the most highly conserved prokaryotic transporter of Fe²⁺, but its mechanism remains to be fully characterized. Most Feo systems are composed of two proteins: FeoA, a soluble SH3-like accessory protein, and FeoB, a membrane protein that translocates Fe²⁺ across a lipid bilayer. Some bacterial *feo* operons encode FeoC, a third soluble, winged-helix protein that remains enigmatic in function. We previously demonstrated that selected FeoC proteins bind O_2 -sensitive [4Fe-4S] clusters via Cys residues, leading to the proposal that some FeoCs could sense O_2 to regulate Fe²⁺ transport. However, not all FeoCs conserve these Cys residues, and FeoC from the causative agent of cholera (*Vibrio cholerae*) notably lacks any Cys residues, precluding cluster binding. In this work, we determined the NMR structure of *Vc*FeoC, which is monomeric and conserves the helix-turn-helix domain seen in other FeoCs. In contrast, however, the structure of *Vc*FeoC reveals a truncated winged β-sheet in which the cluster-binding domain is notably absent. Using homology modeling, we predicted the structure of *Vc*NFeoB and used docking to identify an interaction site with *Vc*FeoC, which is confirmed by NMR spectroscopy. These findings provide the first atomic-level structure of *Vc*FeoC and contribute to a better understanding of its role vis-à-vis FeoB.

Graphical abstract



Keywords Feo · Ferrous iron transport protein C · Ferrous iron transport protein B · Nuclear magnetic resonance · Helix-turn-helix · [4Fe-4S] cluster

Abbreviations

\boxtimes	Aaron T. Smith smitha@umbc.edu
1	Department of Chemistry and Biochemistry, University

of Maryland, Baltimore County, Baltimore, MD 21250, USA

BACTH	Bacterial adenylate cyclase
	two-hybrid
CV	Column volume
DDM	N-Dodecyl-β-D-maltopyranoside
DtxR	Diphtheria toxin repressor



EcFeoC Escherichia coli FeoC
EDTA Ethylenediaminetetraacetic acid
Fe²⁺ Ferrous iron
Fe³⁺ Ferric iron
ENR Eumarate and nitrate reductase

FNR Fumarate and nitrate reductase
GDI GDP dissociation inhibitor
HSQC Heteronuclear single quantum

coherence

IPTG Isopropyl- β -d-1-

thiogalactopyranoside

KpFeoCKlebsiella pneumoniaeFeoCLTTRLysR transcriptional regulatorMWCOMolecular-weight cutoffNMRNuclear magnetic resonanceNOENuclear Overhauser effectNOESYNuclear Overhauser effect

spectroscopy

PMSF Phenylmethylsulfonyl fluoride RMSD Root-mean-square deviation

SH3 SRC homology 3

SEC Size exclusion chromatography

TEV Tobacco etch virus

Vibrio cholerae FeoB VcFeoB Vibrio cholerae FeoC VcFeoC Vibrio cholerae NFeoB VcNFeoB

XNOE Heteronuclear nuclear Over-

hauser effect

Introduction

Iron is essential for nearly all organisms, as it is required for indispensable cellular processes from electron transport and ATP synthesis to DNA biosynthesis [1, 2]. Given this importance, the acquisition of iron is thus necessary for the survival of virtually every organism. For many pathogenic bacteria, iron is typically obtained from a host as siderophore-bound ferric iron (Fe³⁺), iron protoporphyrin IX (heme), and/or ferrous iron (Fe²⁺), and the acquisition of this element is necessary to establish and to maintain infection [2–7]. Methods of Fe³⁺ and heme acquisition have been well-characterized, but pathways for Fe²⁺ uptake are less well-understood.

The ferrous iron transport system (Feo) is the most conserved and broadly distributed system dedicated to Fe²⁺ transport in prokaryotes [5]; however, the precise mechanism of Feo-mediated iron transport remains unclear. The *feo* operon is generally bipartite and encodes for FeoA, a small (*ca.* 8 kDa), cytosolic SH3-like protein [8–10], and for FeoB, a large (*ca.* 85 kDa) transmembrane protein capable of NTP hydrolysis at its soluble N-terminal domain (typically termed NFeoB) [11]. However, in approximately 13% of bacteria, the *feo* operon is tripartite and additionally encodes

for FeoC, a small (ca. 9 kDa), cytosolic protein [12–14]. Structures of FeoC have demonstrated its architecture to include a trihelical helix-turn-helix (HTH) domain fused to a winged β-sheet, akin to that of the LysR transcriptional regulator (LTTR) family [12, 13, 15]. This structural similarity has led to proposals that FeoC functions in transcriptional regulation, although FeoC does not appear to affect FeoB transcription in *Vibrio cholerae* [14, 16]. Additionally, sequence alignments of FeoC proteins highlight the strong conservation of Cys residues within the winged β-sheet, which initially suggested an iron-dependent function of FeoC that could be similar to the iron-sensing diphtheria toxin repressor (DtxR) [17, 18].

Our laboratory recently determined that Escherichia coli and Klebsiella pneumoniae FeoCs (Ec- and KpFeoC, respectively) bind [4Fe-4S] clusters using their Cys-rich winged β -sheet [18, 19]. Although the specific impact of cluster binding on iron transport is currently unknown, we demonstrated that this cluster binding event induces conformational changes in FeoC, which we posited could trigger FeoC-mediated regulation of Feo function, perhaps through interactions with FeoB at its cytosolic domain [19]. Notably, an X-ray crystal structure of the N-terminal domain of FeoB (NFeoB) from K. pneumoniae in complex with KpFeoC has been determined (PDB ID 4AWX; [12]) but the winged β-sheet including its [Fe-S] cluster-binding domain was disordered, precluding assignments of protein-protein interactions of this domain. We also demonstrated that the [4Fe-4S] cluster rapidly degrades upon O₂ exposure, which led to the hypothesis that FeoC may regulate Feo function by sensing O₂ at the [Fe-S] cluster, similar to the fumarate and nitrate reductase (FNR) response regulator [19–21]. Unfortunately, this rapid reactivity in the presence of minute amounts of O₂ made characterizing the structure of the [4Fe-4S] clusterbound form of FeoC difficult even under anoxic conditions. However, some FeoC proteins, including V. cholerae FeoC (VcFeoC), are required for iron transport but do not feature the Cys residues necessary for [Fe-S] cluster-binding based on sequence predictions [14, 22, 23]. Thus, we propose that VcFeoC may belong to a class of FeoC proteins that do not require [Fe-S] cluster-binding and may not be iron-regulated directly but could maintain a state of constitutive activity in their interactions with FeoB [14].

It is plausible that the proposed constitutive activity of Cys-lacking FeoCs may be attributed to structural differences relative to Cys-rich FeoC proteins; however, no structural studies or structural predications of Cys-lacking FeoC are available to date. To this end, we employed solution NMR spectroscopy to determine the first three-dimensional structure of VcFeoC. Gel filtration and NMR data demonstrate that VcFeoC is monomeric in solution under the conditions employed. Importantly, our new structure shows that VcFeoC bears a HTH domain conserved among FeoCs,



but the winged β -sheet is shortened and compacted relative to other FeoC proteins and does not conserve the [Fe-S] cluster-binding domain. To test whether VcFeoC could bind to VcFeoB in the absence of metal, we orthogonally cloned, expressed, solubilized, and purified intact VcFeoB and performed 2D NMR titration assays. These studies confirmed binding and allowed us to map VcFeoC residues that contribute to the binding interface. Finally, we generated a homology model of the soluble N-terminal domain of VcFeoB (VcNFeoB) and performed docking studies in an effort to identify regions of NFeoB involved with VcFeoC binding. Our findings thus reveal the first structure of VcFeoC and how this small protein uses its truncated winged β -sheet to bind to VcFeoB, lending further insight into the role of FeoC within the Feo system.

Experimental methods

Materials

The codon-optimized genes encoding *Vibrio cholerae* serotype O1 FeoC (*Vc*FeoC; Uniprot identifier C3LP26) and *Vibrio cholerae* serotype O1 (strain M66-2) FeoB (Uniprot identifier C3LP27) were synthesized by GenScript. Materials used for buffer preparation, protein expression, and protein purification were purchased from standard commercial suppliers and were used as received. Isotopically enriched ammonium chloride (¹⁵NH₄Cl) and glucose (globally ¹³C₆-labeled) were purchased from Cambridge Isotope Laboratories and used as received. Detergents were purchased from Sigma-Aldrich, stored at -20 °C, and used as received. D₂O was purchased from MilliporeSigma and used as received.

Expression and purification of VcFeoC

The cloning, expression, and purification of VcFeoC was similar to our previous FeoC preparations [19]. Briefly, DNA encoding the gene for Vibrio cholerae serotype O1 FeoC (VcFeoC; Uniprot identifier C3LP26) with an N-terminal (His)₆ tag, maltose binding protein followed by a Tobacco Etch Virus (TEV)-protease cleavage site (ENLY-FQG) was sub-cloned into a pET45b(+) vector, transformed into chemically competent BL21 (DE3) E. coli cells (MilliporeSigma, Burlington, MA), plated on Luria-Bertani (LB) agar plates containing 100 µg/mL of ampicillin (final concentration), and incubated at 37 °C overnight. A single colony was used to generate large-scale (4×1 L) cell cultures grown in LB supplemented with 100 µg/mL ampicillin. Cells were grown at 37 °C until reaching an OD₆₀₀ of 0.6-0.8 at which point the cells were cold shocked briefly at 4 °C. For isotopically enriched samples, a 100-mL LB starter culture treated with 100 µg/mL of ampicillin was grown at 30 °C overnight and was used to inoculate 4×1 L of M9 minimal medium containing ¹⁵NH₄Cl and/or ¹³C₆-glucose (Cambridge Isotope, Tewksbury, MA, USA). The cells were grown in this isotopically enriched minimal media at 37 °C and shaken at 200 rpm until the OD₆₀₀ reached 0.6-0.8 before a brief cold shock at 4 °C. Both natural abundance and isotopically enriched samples were treated with isopropyl-β-D-1-thiogalactopyranoside (IPTG) to a final concentration of 1 mM and incubated at 18 °C with shaking at 200 rpm for 16-20 h before harvesting by centrifugation at 4800×g, 10 min, 4 °C. Cell pellets were resuspended in resuspension buffer (50 mM Tris, pH 7.5, 200 mM NaCl, 5% v/v glycerol), treated with approximately 50–100 mg of solid phenylmethylsulfonyl fluoride (PMSF), and lysed by microfluidization (Microfluidics, Westwood, MA, USA). The lysate was clarified by ultracentrifugation at $163,000 \times g$ for 1 h at 4 °C. The supernatant was applied to two tandem 5-mL MBPTrap HP columns (Cytiva, Marlborough, MA) and purified as previously described [19]. Fractions containing the target protein were concentrated using a 15-mL Amicon with 30-kDa molecular weight cutoff (MWCO) spin concentrator, buffer exchanged into TEV-protease cleavage buffer (50 mM Tris, pH 8.0, 200 mM sodium chloride, 5% v/v glycerol, 1 mM TCEP, 0.5 mM ethylenediaminetetraacetic acid (EDTA)), and concentrated to 1 mL. The concentrated sample was treated with TEV protease and rocked at 4 °C overnight. The TEV-treated sample was purified by size-exclusion chromatography (SEC) using a 120-mL Superdex 75 column equilibrated with SEC buffer (25 mM Tris, pH 7.5, 100 mM sodium chloride, 5% v/v glycerol); cleaved, purified VcFeoC was concentrated using a 15-mL 3-kDa MWCO spin concentrator. This purification approach yielded ca. 1–3 mg VcFeoC L⁻¹ of cell culture. Protein purity was assessed using 20% SDS-PAGE.

NMR spectroscopy of VcFeoC

Each NMR sample contained ca. 2 mg of protein and was prepared in 50 mM of sodium phosphate (pH 6.0) containing 5 mM of NaCl with either 10% or 99% v/v D₂O. Samples prepared in 99% D₂O were exchanged from H₂O using a PD-10 desalting column (Cytiva, Marlborough, MA). The PD-10 column was treated with 1.5 CVs of D_2O_2 equilibrated with 1.5 CVs of NMR buffer prepared in D₂O (50 mM sodium phosphate, pD 6.0, 5 mM NaCl), and eluted using 2 CVs of buffer. NMR datasets were acquired at 25 °C on a Bruker 600 MHz spectrometer equipped with a cryogenic probe. Heteronuclear single quantum coherence (HSOC) experiments were used to establish that VcFeoC was folded and served as a basis for protein backbone assignments. Standard triple resonance experiments (CBCA(CO) NH, HNCACB, HNCO, and HN(CA)CO) were collected to assign the protein backbone [24–27]. A series of two-,



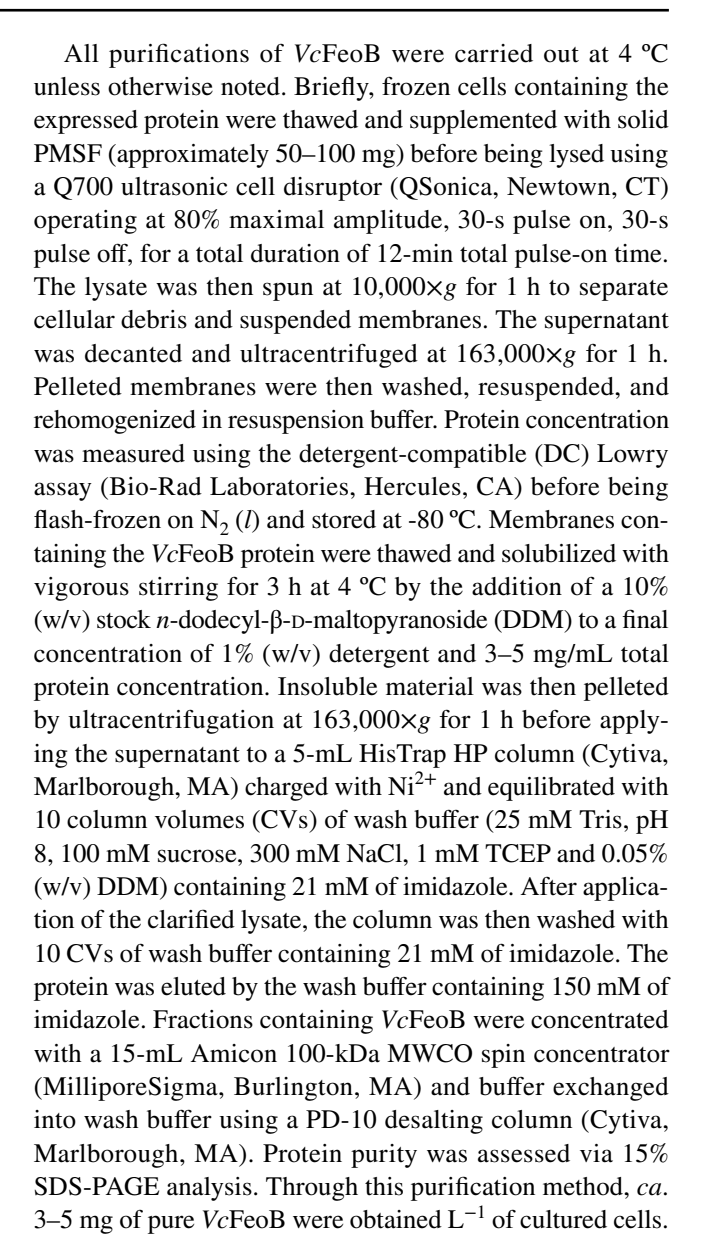
three-, and four-dimensional nuclear Overhauser effect spectroscopy (NOESY) data were collected for combinations of natural abundance and isotopically labeled (¹⁵N, ¹³C, and ¹⁵N/¹³C) protein samples. Protein dynamics were evaluated by ¹H-¹⁵N heteronuclear nuclear Overhauser effect (XNOE) analysis. Data were processed with NMRPipe/nmrDraw or NMRFx and analyzed using NMRViewJ [28–31].

Structural calculations

Structural calculations in torsion angle space were carried out using CYANA [32]. Upper interproton distance limits of 2.7, 3.3, and 5.0 Å were used for NOE cross-peaks of strong, medium, and weak intensities, respectively. Appropriate corrections of interproton distance limits were made for pseudoatoms. The TALOS + Server was used to determine dihedral restraints that were incorporated into structural calculations based on amide proton, amide nitrogen, $H\alpha$, $C\alpha$, $C\beta$, and carbonyl carbon chemical shifts [33]. Hydrogen bond restraints employed in the calculations were determined based on secondary structure assignments given by the $C\alpha$ chemical shift indices and strong NOE patterns diagnostic of the relevant structural elements [34]. PyMOL was employed to prepare structural figures [35]. The atomic coordinates for VcFeoC were deposited in the RCSB database (PDB ID 7U37). NMR chemical shifts and corresponding structure refinement parameters were deposited in the BMRB database (BMRB accession number 30995).

Expression and purification of VcFeoB

The gene encoding for the Vibrio cholerae serotype O1 (strain M66-2) FeoB protein (Uniprot identifier C3LP27) was engineered to contain a C-terminal TEV-protease cleavage site (ENLYFQS) followed by a (His)₆ tag for affinity chromatography purification and subcloned into the pET-21a(+) expression plasmid. This plasmid was transformed into chemically competent BL21 (DE3) E. coli expression cells similar to the MBP-VcFeoC construct. Large-scale expression of the protein was accomplished in 12 baffled flasks charged with 1 L of modified Terrific Broth supplemented with 100 µg/mL of ampicillin. Growth was carried out at 37 °C with shaking at 200 rpm and monitored until an OD₆₀₀ of 1.5–1.75 was reached. Flasks containing cells and media were then cold-shocked at 4 °C before inducing protein expression with the addition of IPTG to a final concentration of 1 mM. Protein expression was carried out at 18 °C with shaking of 200 rpm overnight. After 18–20 h, the cells were harvested by centrifugation at $4800 \times g$, 12 min, 4 °C. Cell pellets were resuspended in resuspension buffer (25 mM Tris, pH 7.5, 100 mM sucrose) and flash-frozen in $N_2(l)$ before storage at -80 °C.



Titration of VcFeoB into VcFeoC

Purified VcFeoB and VcFeoC samples were buffer exchanged into the VcFeoB wash buffer (25 mM Tris, pH 8, 100 mM sucrose, 300 mM NaCl, 1 mM TCEP and 0.05% (w/v) DDM). HSQC spectra were collected as VcFeoB was titrated into 100 μ M VcFeoC samples at stoichiometric (mole/mole) ratios of 0:1, 0.25:1, 0.5:1, and 1:1. Protein precipitation was observed at stoichiometric ratios greater than 1:1, preventing acquisition of further titration datapoints. Data were processed using NMRFx [29].

Predicted docking model of VcNFeoB and VcFeoC

A homology model of *Vc*NFeoB was predicted by using ColabFold [36], which applies the AlphaFold2 structural



prediction approach using MMseqs2 and HHSearch [37]. Docking studies were carried out for the lowest-energy predicted model in combination with the NMR structure of *Vc*FeoC by utilizing the ClusPro online server without modification to the default settings and restraints [38, 39]. The selected docking model chosen was that with the lowest balanced, weighted score that was also consistent with the NMR titration data.

Results

Expression, purification, cleavage, and isolation of VcFeoC

The expression, purification, cleavage, and isolation of untagged VcFeoC from the MBP-tagged construct was carried out similarly to previously described approaches for E. coli and K. pneumoniae FeoC proteins (EcFeoC and KpFeoC, respectively) (Fig. S1) [19]. Specific deviations from the earlier reported methods included: (1) isolation of VcFeoC from the tagged protein by carrying out the Tobacco Etch Virus (TEV)-protease cleavage reaction at 4 °C instead of room temperature to maintain solubility and (2) purification in the absence of reducing agent given that VcFeoC lacks redox-sensitive Cys residues unlike Ec- and KpFeoC. This approach gave rise to yields of ca. 1–3 mg of highly pure protein L^{-1} of cell culture (Fig. S1). Notably, some crystallographic studies of Feo structural elements suggest that NFeoB is trimeric [40], and homology modeling indicates that the Feo system is only operative in an oligomerized, trimeric form [41]; however, we see no evidence for formation of trimeric VcFeoC, and this protein behaves as a monomer in solution based on data from gel filtration experiments (Fig. S1) and NMR analyses (vide infra). These results are consistent with previous results from our laboratory on NFeoAB (a fusion between FeoA and NFeoB), FeoA, and FeoC, which all appear as predominately monomeric species in our hands when studied as isolated proteins [19].

Secondary structure of VcFeoC

Due to the small nature and good accumulation of recombinant VcFeoC, nuclear magnetic resonance (NMR) spectroscopy was employed for structural and dynamics analyses. Gel filtration profiles under NMR conditions indicated that VcFeoC was monodisperse and monomeric (Fig. S1B), consistent with previous findings reported for FeoC proteins [13, 19]. High-quality 2D $^{1}H-^{15}N$ heteronuclear single quantum coherence (HSQC) spectra were acquired for purified VcFeoC (Fig. 1A), which demonstrated well-dispersed amide signals indicative of folded protein [42]. Although the ^{1}H and ^{15}N chemical shifts were generally insensitive to

protein concentration (from 100 to 700 μ M) and sample pH (6.0–8.0) (data not shown), backbone amide assignments were made at pH 6.0 due to optimal long-term protein stability and a decreased $^{1}H^{-2}H$ exchange of amide protons [43]. The established NMR conditions allowed for assignment of all backbone amide signals except for that of Val⁶¹ (99% completion).

To determine the secondary structure of VcFeoC, the Cα chemical shift indices (CSI) were analyzed based on assignment of triple resonance spectra (Fig. 1B, C) [44]. This analysis indicated that VcFeoC is composed of three α -helices (α 1, Leu⁴ to Ser¹³; α 2, Arg¹⁹ to Phe²⁶; α 3, Glu³⁰ to Lys⁴²) and two β -strands (β 1, Arg⁴⁸ to Ile⁵²; β 2, Val⁶¹ to Met⁶⁵), the latter of which are linked to form a short winged β hairpin terminating at an unstructured, dynamic C-terminal tail. Interestingly, negative Cα CSI values at residues immediately preceding the start of $\alpha 2$ (Thr¹⁸) and the start of $\alpha 3$ (Ser²⁹) indicated the presence of N-terminal α -helix capping [45, 46], a structural feature that has been shown to impart additional stability to helices [47]. To characterize further the architecture of VcFeoC, heteronuclear ¹H-¹⁵N NOE (XNOE) data (Fig. 1C, bottom) were acquired. These data offered insight into the backbone dynamics and internal mobility for each signal, where XNOE measurements below ca. 0.8 are indicative of flexibility [48]. The XNOE analysis shows that VcFeoC is largely structured except for three short linkers (Lys¹⁴ to Thr¹⁸, Arg²⁵ to Ser²⁹, and Lys⁴³ to Ser⁴⁷), the β hairpin wing residues (Asn⁵³ to Arg⁶⁰), and the C-terminus (Asn⁶⁶ to Met⁷⁷). Taken together, the XNOE findings both agree with the secondary structure determined from the Ca CSI data and are in general agreement with the structural architecture of previously studied FeoC proteins.

Tertiary structure of VcFeoC

In order to determine the tertiary structure of VcFeoC, ¹⁵N-and ¹⁵N/¹³C-isotopically enriched VcFeoC samples were prepared, and 3D ¹⁵ N-edited nuclear Overhauser effect (NOE), 4D ¹⁵N/¹³C-, and ¹³C/¹³C-edited NOE NMR spectra were acquired [49–52]. After data acquisition, structural calculations were carried out using a total of 648 interproton distance restraints derived from NOE data, 128 hydrogen bond restraints determined based on NOE cross-peak patterns, and 86 dihedral restraints based on backbone chemical shifts (Table 1). An ensemble of 20 refined structures with the lowest target function of 0.005 ± 0.002 Å² was generated for VcFeoC, and this ensemble exhibited good convergence based on root-mean-square deviations (RMSDs) of 0.12 ± 0.04 Å² for backbone heavy atoms (Fig. 2; Table 1).

The tertiary structure of VcFeoC adopts a winged helixturn-helix (HTH) structure featuring a three-helix bundle and a two-stranded antiparallel β -sheet that is connected by an unstructured wing. Long-range NOEs indicate that the



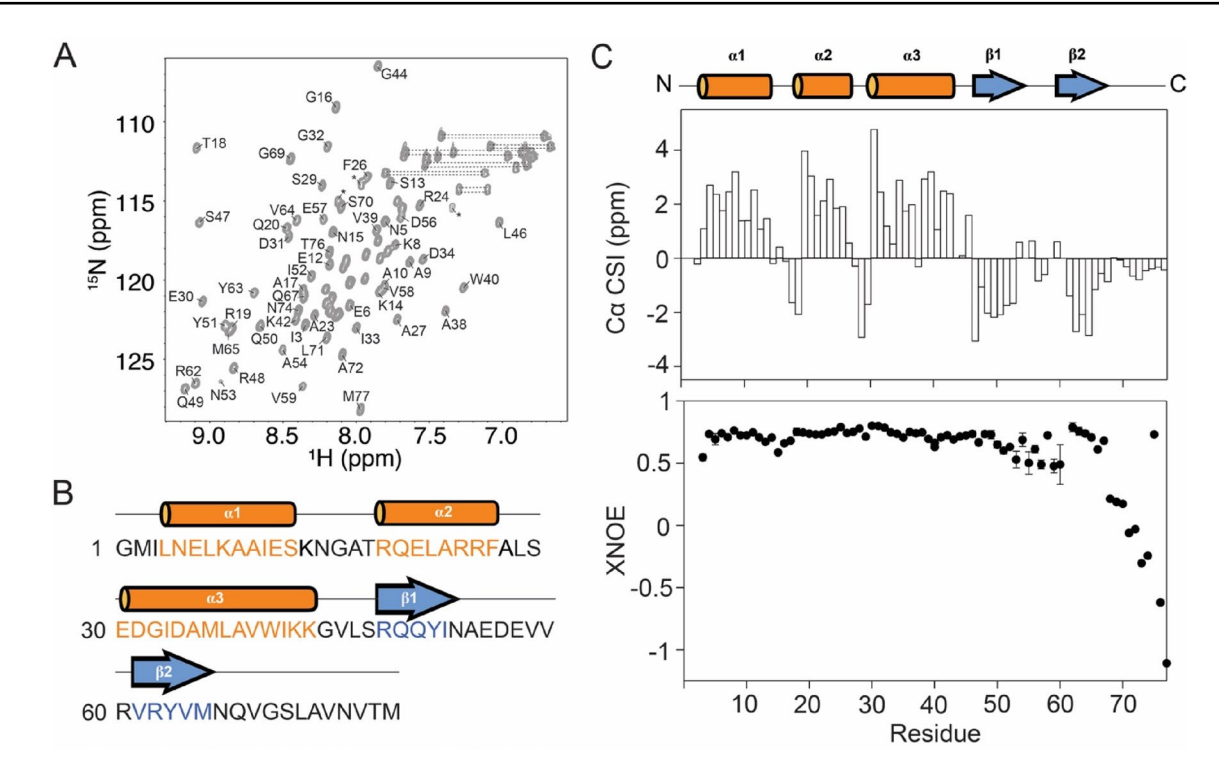


Fig. 1 Secondary structure determination of VcFeoC. **A** Assigned $^1H^{-15}N$ HSQC NMR spectrum of 300 μM VcFeoC at 298 K (50 mM sodium phosphate, pH 6.0, 5 mM NaCl, 10% v/v D_2O). Assignments are generally explicit for residues in the less-crowded regions. Dashed lines represent signals corresponding to Asn and Gln side chains. Asterisks represent signals from Arg side chains. **B** Amino acid sequence of VcFeoC mapped with a cartoon of the corresponding secondary structure of each region. Residues belonging to α-helices are highlighted in orange (α labels) and include the following regions: Leu⁴ to Ser¹³ (α1), Arg¹⁹ to Phe²⁶ (α2), and Glu³⁰ to Lys⁴² (α3). The two-stranded β-sheet (β labels; blue) is composed of residues Arg⁴⁸ to Ile⁵² (β1) and Val⁶¹ to Met⁶⁵ (β2). Note: a single additional Gly

residue at the N-terminus is present as a result of the TEV cleavage reaction. C. NMR chemical shift indices for backbone $C\alpha$ atoms of VcFeoC (top panel); positive values represent α -helical regions, negative stretches represent β -strand residues, and near zero values indicate unstructured and/or random coil regions. $^1H^{-15}N$ heteronuclear NOE (XNOE) data (bottom panel) indicate that VcFeoC is largely structured with the exception of dynamic linkers (Lys 14 to Thr 18 , Arg 25 to Ser 29 , and Lys 43 to Ser 47), the dynamic wing region (Asn 53 to Arg 60), and the C-terminal tail (Asn 66 to Met 77). The amide signal of Val 75 is overlaid with that of Glu 21 (α 2) and therefore gives an XNOE more consistent with a structured element. Error bars represent the standard error associated with each measurement

hydrophobic core of VcFeoC is composed of residues from $\alpha 1-3$ (Leu⁷, Leu²², Ala²³, and Ile³³) and $\beta 2$ (Val⁶⁴) (Fig. 2B, C). In order to quantify the similarity among VcFeoC and other structurally characterized FeoCs, Ca RMSDs were determined of the following: KpFeoC isolated from the X-ray crystal structure of KpFeoC complexed with the N-terminal domain of KpFeoB (KpNFeoB) (1.793 Å; 29 $C\alpha s$) [12], apo KpFeoC (1.770 Å; 22 $C\alpha s$) [13], and EcFeoC(1.595 Å; 30 Cαs) (Table 2). Superpositioning of VcFeoC upon these FeoC homologs highlights the similarity of the gross tertiary structure and, particularly, the conserved HTH domain (Fig. 3). Notably, the main structural differences among FeoCs are variations in the length of the β -strands, the extent of the β-sheet length, and the diversity in the length of the unstructured wing. Intriguingly, whereas both Ec- and KpFeoC have long, Cys-rich wings that serve to bind [4Fe-4S] clusters under anoxic conditions [18, 19], VcFeoC features a shorter wing lacking Cys residues that cannot bind an [Fe-S] cluster. Despite this change, the wing of VcFeoC is still quite dynamic, although it is incapable of sampling as much three-dimensional space as Ec- or KpFeoC wings, due to the size differences. It is possible that this shorter wing region of VcFeoC may be more constrained in space and may actually mimic the cluster-bound forms of Ec/KpFeoC, which are known to be more compact [19].

Interactions between VcFeoB and VcFeoC

Previous work by Hung and coworkers demonstrated the formation of a tight complex between KpFeoC and the guanine dissociation inhibitor (GDI) domain of KpNFeoB, suggesting a role for FeoC in the direct regulation of Fe²⁺ transport [12]. However, these studies were carried out with apo KpFeoC, and the dynamic wing region was unresolved in the electron density; whether the cluster-bound form were capable of binding to KpNFeoB was not explored. Moreover, these studies were unfortunately limited in that KpFeoC was only tested for interactions with the soluble N-terminal



Table 1 Structural restraints and refinement statistics for VcFeoC

NMR-derived restraints	
Intraresidue	319
Sequential $(i-j =1)$	216
Medium/long range $((i-j >1)$	113
Hydrogen bonds	128
Dihedral angle restraints	86
Total restraints	862
Average restraints per residue	11.3
Residual restraint violations	
CYANA target function	$0.00526 \pm 0.00189 \text{ Å}^2$
Maximum violations	
Upper limits	$0.0021 \pm 0.0006 \text{ Å}^2$
Lower limits	$0.0002 \pm 0.00004 \text{ Å}^2$
Van der Waals	$0.04 \pm 0.01 \text{ Å}^2$
Torsion angles	0.0189 ± 0.0065 rad
Structure convergence	
Pairwise rms deviations	
Backbone heavy atoms	$0.12 \pm 0.04 \text{ Å}$
All heavy atoms	$1.12 \pm 0.18 \text{ Å}$
Ramachandran analysis	
Most favored regions	91.55%
Additional allowed regions	5.63%
Generously allowed regions	2.82%

domain of FeoB, not the intact membrane protein. In contrast, bacterial adenylate cyclase two-hybrid (BACTH) assays conducted by Weaver et al. indicated interaction of intact, full-length *Vc*FeoB and *Vc*FeoC under in vivo conditions [14]. Variant studies suggested that the interactions occurred between the N-terminal region of *Vc*FeoB and residues Glu²⁹ and Met³⁵ of *Vc*FeoC [14], but a direct observation of these interactions had not been determined.

Thus, we sought next to determine whether VcFeoC binds to full-length VcFeoB in vitro and, if so, to identify the binding interface of VcFeoB-VcFeoC, which could inform previous in vivo immunoprecipitation findings [22]. However, probing these interactions in vitro required the nontrivial preparation of large amounts of full-length VcFeoB. After multiple optimization attempts, suitable heterologous expression of VcFeoB featuring a C-terminal (His)₆ tag was achieved. Solubilization in *n*-dodecyl-β-D-maltoside (DDM) and subsequent purification reproducibly resulted in the isolation of 2–3 mg of highly pure VcFeoB L⁻¹ of cells culture (Fig. S2). To determine whether VcFeoC interacts with the intact VcFeoB in vitro, 2D ¹H-¹⁵N HSQC NMR spectra of VcFeoC were acquired as VcFeoB was titrated into various stoichiometric ratios (mole/mole) of VcFeoC (Fig. 4). Given the large size of VcFeoB (ca. 85 kDa) incorporated into DDM micelles (ca. 70 kDa), formation of the DDM-VcFeoB-FeoC complex (ca. 164 kDa) results in a decreased

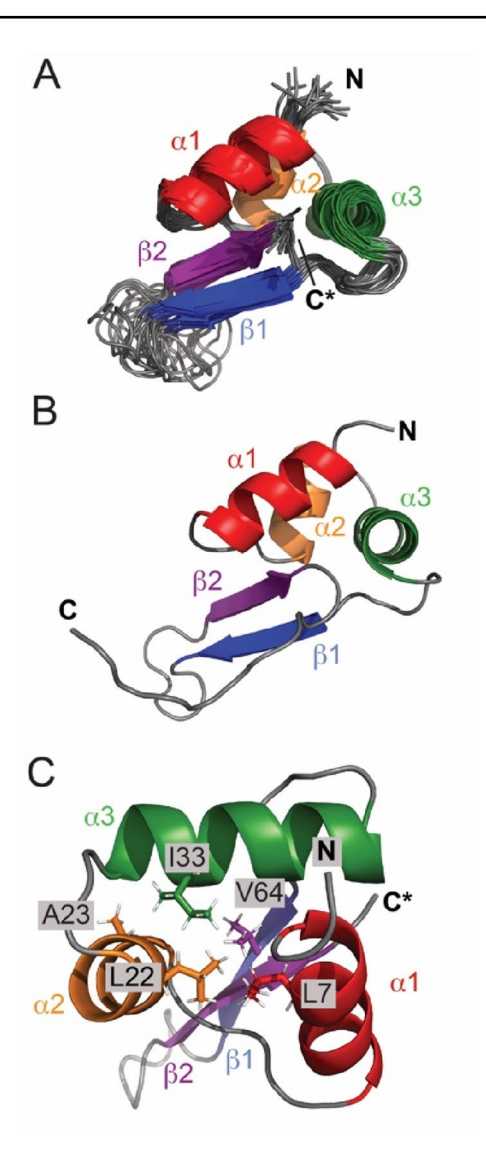


Fig. 2 NMR structure of VcFeoC. A Superposition of the 20 lowest-energy refined structures of VcFeoC. The structured regions are Leu⁴ to Ser¹³ (α 1; red), Arg¹⁹ to Phe²⁶ (α 2; orange), Glu³⁰ to Lys⁴² (α 3; green), Arg⁴⁸ to Ile⁵² (β 1; blue), and Val⁶¹ to Met⁶⁵ (β 2; purple). The ribbon representations include Gly¹ through Gln⁶⁷ to demonstrate the globular portion of the structure, but the dynamic C-terminal tail is truncated for clarity (represented by C*). **B** Ribbon diagram of the full-length, lowest-energy target function structure of VcFeoC. **C** The hydrophobic core of VcFeoC includes residues Leu⁷, Leu²², Ala²³, Ile³³, and Val⁶⁴, which combined hold together the helix-turn-helix motif. The N- and C-termini are represented by 'N' and 'C' labels, respectively. Images in which the dynamic, unstructured C-terminus is truncated for figure clarity are labeled with 'C*.' Cartoons are representative of backbone traces of VcFeoC

NMR signal of the observed (unbound) *Vc*FeoC (*ca.* 9 kDa) [53, 54]. The *Vc*FeoB–*Vc*FeoC complex is not detected as large DDM micelles tumble slowly, and the NMR signal is further masked as a result of the low protein-to-detergent ratio [55]. Importantly, a control detergent-to-*Vc*FeoC titration was also performed to ensure that the decreased *Vc*FeoC



Table 2 $C\alpha$ RMSD s of the NMR-derived structure of VcFeoC and other bacterial FeoC structures

Protein	PDB ID	RMSD (Å) ^a
Escherichia coli FeoC	1XN7	1.595
Klebsiella pneumoniae FeoC	2K02	1.770
Klebsiella pneumoniae FeoC (NFeoB-bound)	4AWX	1.793

 $^{^{}a}$ Root-mean-square deviation calculated between $C\alpha$ atoms of matched residues

signal intensity was the result of binding to VcFeoB and not adventitious interactions with DDM micelles (Fig. S3). The overlaid HSQC data indicate that VcFeoC binds VcFeoB using the following regions on VcFeoC: Asn¹⁵, Gly¹⁶, and Thr¹⁸ of the HTH domain; Glu³⁰ of linker 2 (analogous to Glu²⁹ identified in the previous BACTH studies [14]); Asp³⁴ and Ala³⁸ to Trp⁴⁰ of α 3; Leu⁴⁶ and Ser⁴⁷ of linker 3; Arg⁴⁸ to Gln⁵⁰ and Arg⁶² to Val⁶⁴ β -sheet; and Glu⁵⁷ of the wing (Fig. 4). We failed to observe any sign of interactions with the analogous Met³⁵ in the previous BACTH studies. Attempts to titrate VcFeoB into VcFeoC beyond a 1:1 (mole/mole) ratio resulted in sample precipitation.

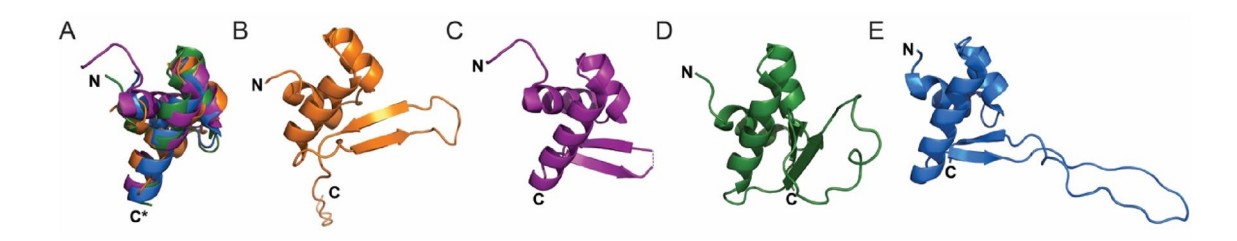


Fig. 3 Comparisons of structurally characterized FeoC proteins. **A** Overlaid, truncated structures (residues 1–45) of the lowest target function NMR-derived *Vc*FeoC (orange; PDB ID 7U37), the crystal structure of *Klebsiella pneumoniae* FeoC (*Kp*FeoC) isolated from the *Kp*FeoC-*Kp*NFeoB complex (purple; PDB ID 4AWX), apo *Kp*FeoC (green; PDB ID 2K02), and *Escherichia coli* FeoC (*Ec*FeoC, blue; PDB ID 1XN7). The superpositioning of these structures demonstrates the similarity within the conserved three-helix bundle (approximately residues 1–45 of each protein). Ribbon diagrams of the full-

length NMR structure of VcFeoC (**B**), crystallized KpFeoC bound to KpNFeoB (**C**), the NMR structure of apo KpFeoC (**D**), and the NMR structure of apo EcFeoC (**E**). These comparisons illustrate the heterogeneity observed within the winged regions of the winged-helix motif among FeoC proteins. The N- and C-termini are represented by 'N' and 'C' labels, respectively. Images in which the C-terminus is truncated for figure clarity are labeled with 'C*.' Cartoons are representative of backbone traces of FeoC proteins

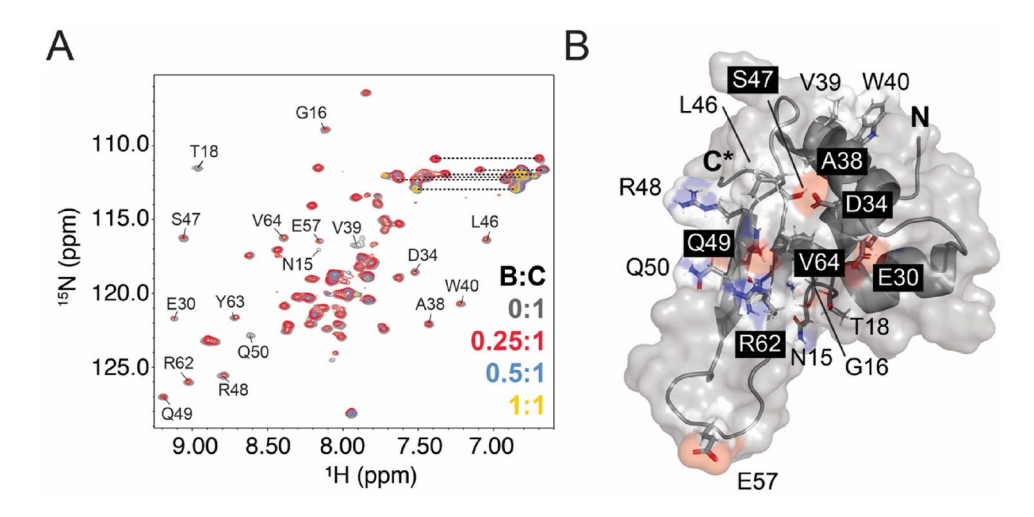


Fig. 4 V_c FeoC binds to intact V_c FeoB. A Overlaid 1 H- 15 N HSQC spectra of V_c FeoB titrated into 100 μ M V_c FeoC (gray) at stoichiometric ratios (mole/mole) of 0.25:1 (red), 0.5:1 (blue), and 1:1 (yellow) at 298 K (50 mM Tris, pH 8.0, 100 mM sucrose, 200 mM NaCl, 0.05% dodecyl- β -D-maltoside, 1 mM TCEP). Micelle-associated V_c FeoB is not detected given its large size, and the broadened loss of V_c FeoC signals represents formation of the V_c FeoB- V_c FeoC complex. Labels are included and correspond to V_c FeoC signals that broaden the most rapidly due binding at the V_c FeoB/ V_c FeoC interface. Dashed lines represent Asn and Gln side chain signals. **B** A surface and cartoon repre-

sentation of the truncated, lowest-energy structure of VcFeoC (residues 1–67) indicating that residues within the helix-turn-helix (HTH) region (Asn¹⁵, Gly¹⁶, and Thr¹⁸), linker 2 (Glu³⁰), α 3 (Asp³⁴, Ala³⁸-Trp⁴⁰), linker 3 (Leu⁴⁶ and Ser⁴⁷), β -sheet (Arg⁴⁸-Gln⁵⁰, Arg⁶²-Val⁶⁴), and wing (Glu⁵⁷) broaden rapidly due to interaction with VcFeoB. Labels are included for all residues for which broadened signals are observed except for Tyr⁶³ that is on the opposite face of β 2. The N- and truncated C-terminus is represented by 'N' and 'C*' labels, respectively



As we presumed that VcFeoC interacts with the N-terminal domain of VcFeoB (VcNFeoB) based on previous data [12], but our NMR titrations only give us a spectroscopic and structural handle for VcFeoC, we then sought to understand the interaction between VcFeoC and VcNFeoB better through modeling approaches. As several structures of NFeoB homologs exist in the PDB, we determined a homology model of VcNFeoB, and we used the lowest-energy model to dock VcFeoC onto VcNFeoB. Several docking models predicted interactions in a similar orientation to those shown in Fig. 5A, demonstrating that electrostatic and hydrophobic interactions reinforce binding between Switch I/Switch II and the GDI domains of VcNFeoB with the winged β -sheet of VcFeoC, consistent with our NMR findings (vide supra).

These results are similar to those observed in the *KpNFeoB/KpFeoC* complex X-ray crystal structure (PDB ID 4AWX; Fig. 5 B, C). Unfortunately, in that structure, the asymmetric unit (ASU) of this complex was ambiguous and suggested that *KpFeoC* could interact with *KpN-FeoB* via hydrogen bonding, electrostatic interactions, and interactions of hydrophobic residues between two different regions: the GDI domain on a single *KpNFeoB* protomer and the Switch II region of the neighboring *KpNFeoB* protomer (Fig. 5B) [12]. Thus, our modeling data suggest that both could be operative, at least for *VcFeoC*, which may represent a constitutive mimic of the holo, [Fe-S] cluster-bound form of FeoC, which was absent from the *K. pneumoniae* complex structure.

Discussion

Although the function of FeoC remains disputed, this poorly conserved protein appears to serve a function that is important for Fe²⁺ transport in several γ -proteobacteria [14, 23, 56]. Many of these organisms are pathogenic prokaryotes, including notable problematic organisms such as Salmonella enterica [56, 57], V. cholerae [14], and K. pneumoniae [12]. Our laboratory has demonstrated that the role of some FeoCs is likely dependent on the binding of an oxygen-sensitive [Fe-S] cluster in the dynamic wing regions of FeoC [19], contrasting earlier studies suggesting that these clusterbinding FeoCs could be oxygen-tolerant [18]. Studies of S. enterica FeoC further confirm that FeoC is oxygen-sensitive and could regulate FeoB levels under changing metabolic conditions [57]. Unfortunately, the oxygen-sensitive nature of the [Fe-S] cluster makes structural determination of cluster-replete FeoCs challenging [19]. However, some FeoC proteins in pathogens like V. cholerae lack the necessary cluster-binding residues, prohibiting [Fe-S] cluster binding, yet these proteins remain functionally important [14, 19, 22]. These observations have led us to hypothesize that the

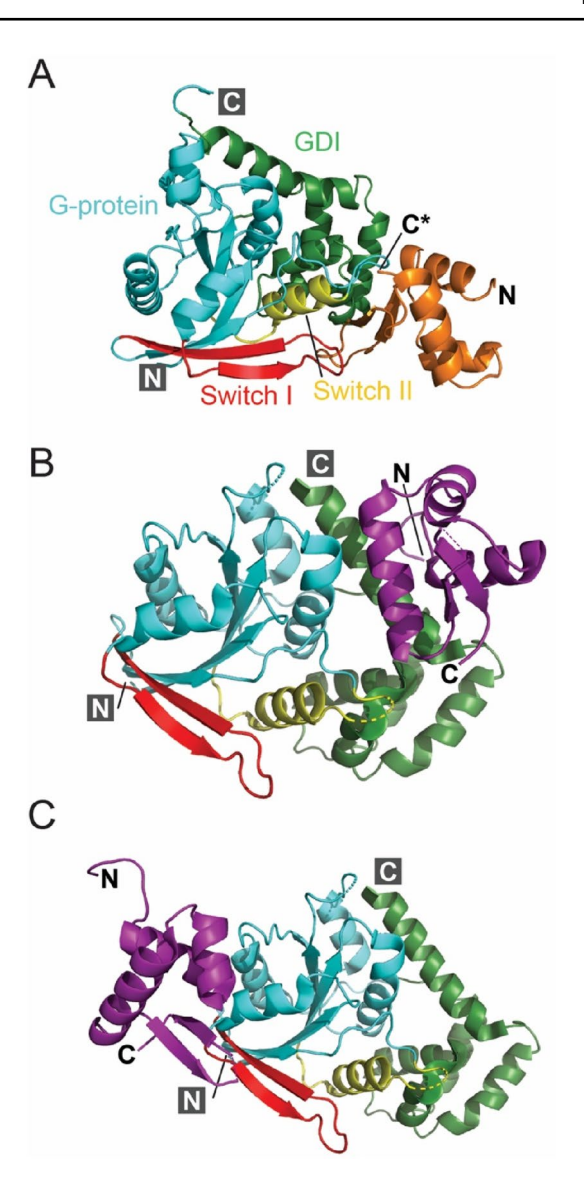


Fig. 5 VcFeoC-VcNFeoB docking model and its comparison to the KpFeoC-KpNFeoB co-crystal structure. **A** Docking studies of VcFeoC (orange) and the homology model of VcNFeoB suggest interactions of the VcFeoC β-sheet and wing with Switch I (red), Switch II (yellow), and GDI (green) domains. **B** Studies of KpFeoC (purple) co-crystallized with KpNFeoB (PDB ID 4AWX) indicate that KpFeoC α3 interacts with NFeoB by means of hydrogen bonds, salt bridges, and hydrophobic interactions with the GDI (green) and Switch II (yellow) domains [12]. **C** Extended crystal contacts throughout the crystalline lattice indicate an alternative mode of binding of KpFeoC (purple) to KpNFeoB in which the KpFeoC wing interacts with the Switch I region of KpNFeoB (red). Images in which the dynamic, unstructured C-terminus is truncated for figure clarity are labeled with 'C*.' The G-protein domain is colored in cyan. The N- and C-termini are represented by 'N' and 'C' labels, respectively

functional aspect of FeoC may either be located at a structural site outside of the [Fe-S] cluster-binding residues, or that FeoCs lacking [Fe-S] cluster binding could be constitutively active and always capable of affecting iron transport.



To this end, we determined the NMR structure of VcFeoC, which is generally similar to the previously solved Ec- and KpFeoC structures (Fig. 3 and Table 2). VcFeoC features the conserved N-terminal, trihelical HTH domain but differs at the C-terminal winged β -sheet [12, 13]. Two main differences are observed between VcFeoC and its [Fe-S] cluster-binding homologs: VcFeoC features shorter β-sheet and wing regions and has a long, disordered C-terminal tail (Fig. 3) [13]. In particular, we believe that the observed differences in the winged β-sheet are due to differences in [Fe-S] cluster binding capabilities: Ec- and KpFeoC bind [4Fe-4S] clusters using long, dynamic, Cys-rich wings that undergo conformational changes to accommodate this cofactor [13, 18, 19], whereas VcFeoC does not. We know that [Fe-S] cluster binding in Ec- and KpFeoC results in compaction of structure [19], and we believe that VcFeoC could naturally mimic this more compact structure without the need of [Fe-S] cluster binding in order to affect function via protein-protein interactions.

FeoC is known to interact with other components of the Feo system, although a consensus on function still seems unclear. BACTH assays of the V. cholerae Feo system show that FeoB and FeoC interact [14], and immunoprecipitation studies demonstrate that FeoA, FeoB, and FeoC could form a complex, albeit very large [22]. Interestingly, this work proposed a requirement for FeoA but not FeoC in complex formation and suggested that FeoC could serve to regulate FeoB directly or its protein levels. In S. enterica, FeoC was proposed to protect FeoB from FtsH-mediated proteolysis. However, the decreased levels of SeFeoB were still sufficient for iron transport, indicating that proteolysis protection may not be the primary role of SeFeoC [56]. It has also been suggested that SeFeoC is under proteolytic regulation by the Lon protease, as SeFeoC was rapidly degraded by Lon proteases in high-oxygen conditions, suggesting that the putative [Fe-S] plays a role in protecting SeFeoC from degradation [57]. However, given that VcFeoC does not have [Fe-S] cluster binding capabilities, it is unknown whether this function is conserved, at least in V. cholerae. In contrast, BACTH assays implicated two VcFeoC residues (Glu²⁹ and Met³⁵) in giving rise to interactions with FeoB, but other participating residues were not identified.

Although the size of the *Vc*FeoB-micelle complex prohibits the determination of the FeoB binding interface via NMR, our docking studies suggest that a cavity formed by the GDI domain and the Switch I/II regions of *Vc*NFeoB acts as the binding receptacle for *Vc*FeoC via residues Gly³⁴, Thr³⁶, Asp⁷², Ile⁷⁵, Arg⁷⁸, and Lys²²⁰ on *Vc*NFeoB, which could influence nucleotide hydrolysis. Interestingly, Thr³⁶ in Switch I and Asp⁷² in Switch II were previously reported as necessary for NTPase activity, Fe²⁺ transport, and/or complex formation of FeoA, -B, and -C [22, 58]; however, in vitro findings have demonstrated that FeoC

does not significantly influence NTPase activity of *Vc*FeoB [59]. Considering the in vivo findings that FeoA, FeoB, and FeoC all interact in *V. cholerae* [22], it is plausible that the presence of *Vc*FeoA could facilitate *Vc*FeoB-*Vc*FeoC interactions. In fact, this complex formation could even be nucleotide-mediated, and recent work from our laboratory has shown that FeoA-FeoB interactions can be facilitated by the presence of nucleotide [10]. Ultimately, these events may be related to Fe²⁺ translocation via the transmembrane domain, especially given FeoC's interactions near the GDI domain that links directly to the first transmembrane helix. However, additional mechanistic and structural work is necessary to further probe this hypothesis, which is an exciting future avenue of research.

Supplementary Information The online version contains supplementary material available at https://doi.org/10.1007/s00775-022-01945-4.

Acknowledgements This work was supported by NSF CAREER grant 1844624 (A. T. S. and M. L.), NIH-NIGMS grant R35 GM133497 (A. T. S. and J. B. B.), and in part by NIH-NIGMS grant T32 GM066706 (M. L.). Sequence searches utilized both database and analysis functions of the Universal Protein Resource (UniProt) Knowledgebase and Reference Clusters (http://www.uniprot.org) and the National Center for Biotechnology Information (http://www.ncbi.nlm.nih.gov/). We thank Prof. Michael F. Summers (UMBC) for generous access to NMR facilities, reagents, and technical support.

Declarations

Conflict of interest The authors declare no competing financial interest.

References

- Krewulak KD, Vogel HJ (2008) Biochim Biophys Acta 1778:1781–1804
- Andrews SC, Robinson AK, Rodríguez-Quiñones F (2003) FEMS Microbiol Rev 27:215–237
- Wooldridge KG, Williams PH (1993) FEMS Microbiol Rev 12:325–348
- 4. Skaar EP (2010) PLoS Pathog 6:e1000949
- 5. Brown JB, Lee MA, Smith AT (2021) Biochemistry 60:3277–3291
- Miethke M, Marahiel MA (2007) Microbiol Mol Biol Rev 71:413–451
- Contreras H, Chim N, Credali A, Goulding CW (2014) Curr Opin Chem Biol 19:34–41
- 8. Lau CK, Ishida H, Liu Z, Vogel HJ (2013) J Bacteriol 195:46-55
- 9. Linkous RO, Sestok AE, Smith AT (2019) Proteins 87:897-903
- Sestok AE, Brown JB, Obi JO, O'Sullivan SM, Garcin ED, Deredge DJ, Smith AT (2022) J Biol Chem 298:101808
- Eng ET, Jalilian AR, Spasov KA, Unger VM (2008) J Mol Biol 375:1086–1097
- Hung KW, Tsai JY, Juan TH, Hsu YL, Hsiao CD, Huang TH (2012) J Bacteriol 194:6518–6526
- Hung KW, Juan TH, Hsu YL, Huang TH (2012) J Biomol NMR 53:161–165
- Weaver EA, Wyckoff EE, Mey AR, Morrison R, Payne SM (2013)
 J Bacteriol 195:4826–4835



- 15. Maddocks SE, Oyston PCF (2008) Microbiology 154:3609–3623
- Cartron ML, Maddocks S, Gillingham P, Craven CJ, Andrews SC (2006) Biometals 19:143–157
- D'Aquino JA, Tetenbaum-Novatt J, White A, Berkovitch F, Ringe D (2005) Proc Natl Acad Sci U S A 102:18408–18413
- 18. Hsueh KL, Yu LK, Chen YH, Cheng YH, Hsieh YC, Ke SC, Hung KW, Chen CJ, Huang TH (2013) J Bacteriol 195:4726–4734
- Smith AT, Linkous RO, Max NJ, Sestok AE, Szalai VA, Chacón KN (2019) Biochemistry 58:4935–4949
- Crack JC, Stapleton MR, Green J, Thomson AJ, Le Brun NE (2014) Biochem J 463:83–92
- Sutton VR, Mettert EL, Beinert H, Kiley PJ (2004) J Bacteriol 186:8018–8025
- Stevenson B, Wyckoff EE, Payne SM (2016) J Bacteriol 198:1160–1170
- Sestok AE, Linkous RO, Smith AT (2018) Metallomics 10:887–898
- 24. Grzesiek S, Bax A (1992) J Am Chem Soc 114:6291-6293
- 25. Grzesiek S, Bax A (1992) J Magn Reson 99:201-207
- Kay LE, Ikura M, Tschudin R, Bax A (1990) J Magn Reson 89:496–514
- Clubb RT, Thanabal V, Wagner G (1992) J Magn Reson 97:213–217
- Delaglio F, Grzesiek S, Vuister GW, Zhu G, Pfeifer J, Bax A (1995) J Biomol NMR 6:277–293
- Norris M, Fetler B, Marchant J, Johnson BA (2016) J Biomol NMR 65:205–216
- 30. Johnson BA, Blevins RA (1994) J Biomol NMR 4:603-614
- 31. Johnson BA (2004) Methods Mol Biol 278:313-352
- 32. Güntert P (2004) Methods Mol Biol 278:353-378
- 33. Shen Y, Delaglio F, Cornilescu G, Bax A (2009) J Biomol NMR 44:213–233
- Wüthrich K (1986) NMR of proteins and nucleic acids. Wiley, New York
- DeLano WL (2002) The PyMOL molecular graphics system.
 DeLano Scientific, San Carlos, CA
- Mirdita M, Schütze K, Moriwaki Y, Heo L, Ovchinnikov S, Steinegger M (2021). BioRxiv. https://doi.org/10.1101/2021.08. 15.456425
- 37. Jumper J, Evans R, Pritzel A, Tim G, Figurnov M, Ronneberger O, Tunyasuvunakool K, Bates R, Zídek A, Potapenko A, Bridgland A, Meyer C, Kohl SAA, Ballard AJ, Cowie A, Romera-Paredes B, Nikolov S, Jain R, Adler J, Back T, Petersen S, Reiman D, Clancy E, Zielinski M, Steinegger M, Pacholska M, Berghammer T, Bodenstein S, Silver D, Vinyals O, Senior AW, Kavukcuoglu K, Kohli P, Hassabis D (2021) Nature 596:583–589

- Kozakov D, Hall DR, Xia B, Porter KA, Padhorny D, Yueh C, Beglov D, Vajda S (2017) Nat Protoc 12:255–278
- Kozakov D, Beglov D, Bohnuud T, Mottarella SE, Xia B, Hall DR, Vajda S (2013) Proteins: Struc Funct Bioinform 81:2159–2166
- Guilfoyle A, Maher MJ, Rapp M, Clarke R, Harrop S, Jormakka M (2009) EMBO J 28:2677–2685
- Seyedmohammad S, Fuentealba NA, Marriott RA, Goetze TA, Edwardson JM, Barrera NP, Venter H (2016). Biosci Rep. https:// doi.org/10.1042/BSR20160046
- Breukels V, Konijnberg A, Nabuurs SM, Doreleijers JF, Kovalevskaya NV, Vuister GW (2011) Current protocols in protein science. Wiley, Hoboken, p 17.15.11-17.15.44
- 43. Wuthrich K, Wagner G (1979) J Mol Biol 130:1-18
- 44. Wishart DS, Sykes BD (1994) J Biomol NMR 4:171-180
- 45. Gronenborn AM, Clore GM (1994) J Biomol NMR 4:455-458
- 46. Shen Y, Bax A (2012) J Biomol NMR 52:211–232
- 47. Serrano L, Fersht AR (1989) Nature 342:296–299
- 48. Kay LE, Torchia DA, Bax A (1989) Biochemistry 28:8972–8979
- Kay LE, Clore GM, Bax A, Gronenborn AM (1990) Science 249:411–414
- 50. Kay LE, Ikura M, Bax A (1990) J Am Chem Soc 112:888-889
- Marion D, Driscoll PC, Kay LE, Wingfield PT, Bax A, Gronenborn AM, Clore GM (1989) Biochemistry 28:6150–6156
- Vuister GW, Clore GM, Gronenborn AM, Powers R, Garrett DS, Tschudin R, Bax A (1993) J Magn Reson Ser B 101:210–213
- Ceccon A, D'Onofrio M, Zanzoni S, Longo DL, Aime S, Molinary H, Assfalg M (2013) Proteins 81:1776–1791
- Mercredi PY, Bucca N, Loeliger B, Gaines CR, Mehta M, Bhargave P, Tedbury PR, Charlier L, Floquet N, Muriaux D, Favard C, Sanders CR, Freed EO, Marchant J, Summers MF (2016) J Mol Biol 428:1637–1655
- 55. Privé GG (2007) Methods 41:388-397
- 56. Kim H, Lee H, Shin D (2013) J Bacteriol 195:3364-3370
- 57. Kim H, Lee H, Shin D (2015) J Bacteriol 197:92–98
- Shin M, Mey AR, Payne SM (2019) Proc Natl Acad Sci U S A 116:4599–4604
- 59. Gómez-Garzón C, Payne SM (2020) Metallomics 12:2065-2074

Publisher's Note Springer Nature remains neutral with regard to jurisdictional claims in published maps and institutional affiliations.

